Detection of fecal contamination on apples with nanosecond-scale time-resolved imaging of laser-induced fluorescence

Alan M. Lefcourt, Moon S. Kim, and Yud-Ren Chen

Detection of apples contaminated with feces is a public health concern. We found that time-resolved imaging of apples artificially contaminated with feces allowed optimization of timing parameters for detection. Dairy feces were applied to Red Delicious and Golden Delicious apples. Laser-induced fluorescence responses were imaged by use of a gated intensified camera. We developed algorithms to automatically detect contamination iteratively by using one half of the apples and validated them by applying the optimized algorithms to the remaining apples. Results show that consideration of the timing of fluorescence responses to pulsed-laser excitation can enhance detection of feces on apples.

OCIS codes: 150.3040, 170.0110, 170.6280, 300.2530.

1. Introduction

Feces are the primary source of pathogenic *Escherichia coli* (*E. coli*) contamination of agricultural commodities, and both the Food and Drug Administration[1] and the Food Safety and Inspection Service[2] use the presence of *E. coli* as an indicator of fecal contamination. The adverse health risks of pathogenic organisms originating from feces, including *E. coli* O157:H7, in foods are well documented. The Food and Drug Administration has requested that the U.S. Department of Agriculture develop methods to detect fecal contamination of fruits and vegetables and, in particular, of apples used to make juice. As a consequence, the Instrumentation and Sensing Laboratory was assigned the task of developing instrumentation to detect fecal contamination.

Fluorescence sensing techniques are widely used in a number of scientific applications including cell biology, photochemistry, medicine, and environmental sciences. Plant materials, including leaves and fruits, exhibit fluorescence emissions in the visible region of the spectrum when excited with appropriate radiation. Fluorescence emission peaks (maxima) from these materials are typically observed in the blue, green, red, and far-red regions of the spectrum at approximately 450, 530, 685, and 735 nm, respectively. The authors have demonstrated that feces show similar responses and that responses from feces from different species of agricultural interest are similar.[16]

In prior studies the authors demonstrated that fecal contamination of apples can be detected on the basis of differential fluorescence responses of feces and normal apple surfaces.[13,17] The ultimate goal of the research program is to develop methodologies that can be used for real-time evaluation of apples during processing. In this regard, the authors developed a multispectral laser-induced fluorescence imaging system, which was used to detect fecal contamination of apples.[17,18] The system used a UV pulsed laser to excite samples and an intensified camera to record fluorescence responses. A specific advantage of this pulsed-laser system is that images from samples with low quantum yields can be acquired rapidly regardless of ambient light conditions.

The current study addresses potential methods for increasing the selectivity and specificity of the use of a laser-induced fluorescence imaging system for detecting fecal contamination on apples. The authors previously showed that the maximal fluorescence yield from feces is obtained with an excitation wavelength around 417 nm.[16] In this study the UV pulsed laser was replaced by a pulsed laser with an optical parametric oscillator that allowed one to tune the output wavelength to 417 nm. In addition, it was

The authors are with the Instrumentation and Sensing Laboratory, U.S. Department of Agriculture, Agricultural Research Service, Building 303 Powder Mill Road, Beltsville, Maryland 20705. A. Lefcourt's e-mail address is alefcour@anri.barc.usda.gov.

Received 31 December 2003; revised manuscript received 19 May 2004; accepted 25 October 2004.

hypothesized that consideration of time-dependent differences in fluorescence responses of areas with or without feces treatment might allow for improved detection of contaminated apples. To test this possibility, we used an intensified camera with a gate width of 2 ns to image artificially contaminated apples sequentially by time.

2. Materials and Methods

Serial dilutions of dairy feces were applied to Red Delicious and Golden Delicious apples. We detected contamination sites by taking advantage of differences between fluorescence responses of apple surfaces and of feces. One half of the apples were used to develop detection algorithms. The algorithms were validated with the remaining apples.

A. Apples

The Red Delicious and Golden Delicious apples used in the study were handpicked from crates of tree-run apples at the Rice Fruit Co. (Gardners, Pa.). The apples were stored under commercial conditions in an apple refrigerator maintained at 3 °C. Apples for treatment were selected randomly on the basis of two criteria: first, apples were not damaged and, second, the flesh of the apple was firm with no sign of rot. Feces were applied to 100 apples of each type.

B. Feces Application

Fresh cow feces were collected at the Beltsville Agricultural Research Center dairy. The feces were immediately processed and applied to the apples. We determined dry-matter content of the feces ($14.8 \pm 0.2\%$) by drying three samples to a constant weight in a 95 °C oven. The fresh feces were serially diluted 1:2, 1:20, and 1:200 by weight with double-distilled water. A single 30-μl drop of each of the three dilutions was applied to the cheek surface of individual apples by use of a pipette with one drop per quadrant; the fourth quadrant was not treated. To accommodate particulates in the dilutions, approximately 2 mm were cut off the end of the pipette tip with a razor blade. The drops were applied clockwise in sequence by concentration, and the initial quadrant for application was rotated one quadrant clockwise every fourth apple (Fig. 1).

The last four apples in each group of 100 were handled a little differently than the remainder of the apples. The locations of specific treatment sites on these four apples were rotated apple by apple so that the four application patterns were all represented. These four apples were designed to be potential substitutes if problems occurred with any of the other 96 apples. In actuality, two Red Delicious apples were substituted because one was dropped and because one application site visibly ran, and one Golden Delicious apple was substituted because the application pattern was rotated inappropriately. Thus only 96 apples from each group were actually used for analyses.

Following feces application, the apples were returned to the apple refrigerator. Over the next 24 to 72 h, single trays of a dozen apples were removed for imaging as needed. Two trays were out of the refrigerator at any given time: One tray was in active use while the apples in the second tray were allowed to acclimate to room temperature.

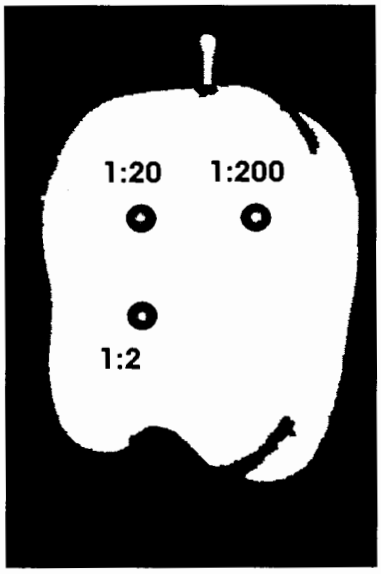

Fig. 1. Application sites for 1:2, 1:20, and 1:200 serial dilutions of dairy feces. The order of the applications followed a clockwise rotation based on concentration. The initial quadrant for application of the 1:2 dilution was incremented one quadrant clockwise every fourth apple.

C. Imaging System

Fluorescence emissions from single apples were acquired by use of a multispectral laser-induced fluorescence imaging system. The light source was a 10-Hz optical parametric oscillator pulsed (~6-ns pulse width) laser (Vibrant VIS; Opotek, Calif.). The laser system provides an output based on the Q switch that can be used to trigger the imaging system. The trigger output can be set to occur within ±100 ns of the actual Q-switch event. The maximum power across most of the frequency range (415 to 650 nm) of the optical parametric oscillator is ~50 mJ per pulse; however, power is lower at the extremes of the operating range. Trials were conducted with 417-nm excitation at a power level of 25 to 30 mJ. A pair of internal lenses expands the beam of the laser to encompass a 12-cm-diameter target area at 150 cm. A Gen II intensified charge-coupled-device (ICCD) camera was used for imaging (IStar; Andor Technology, Mass.; minimum gate width 2 ns, pixel resolution 1024×1024, and effective pixel size $13\ \mu m \times 13\ \mu m$). Attached to the camera was a 25-mm Nikon lens along with a common-aperture multispectral adaptor (MSAI-04; Optical Insights, Ariz.) that uses prisms to create four 512×512 images in separate quadrants of the 1024×1024 camera image. The advantage of this adapter is that a different interference filter can be used for each quadrant. Filter parameters used for this study were

40-nm FWHM at 590 nm (yellow band), 22-nm FWHM at 682 nm (red band), 30-nm FWHM at 700 nm (broad red band), and 10-nm FWHM at 730 nm (far-red band). The camera was positioned at a 5° angle to the laser beam at a distance from the target stage (~100 cm) to allow single apples to be imaged. Preliminary tests of imaging quality indicated that the largest source of variation was the fluorescence responses across individual, untreated apple surfaces and among apples. Second was the variability inherent in using a pulsed laser for illumination; however, averaging responses of eight sequential pulses kept differences in image-to-image illumination to less than 2%. Tests of optical components revealed distinct optical aberrations due to the multispectral adapter at the edges of each of the four imaging quadrants. However, within the center regions used to image apples, responses were near uniform. In practice, no attempt was made to correct images prior to image analyses. The primary reason for this decision was that the variability that can be attributed to the imaging system is minimal, and, as the ultimate goal of the research is the development of a rapid detection system, the computational overhead of an additional correction step is not warranted.

D. Image Acquisition

The camera is controlled and data are collected and analyzed with a personal computer running Microsoft Windows XP Professional and Visual Basic version 6. Image acquisition uses the software development kit provided by Andor Technology to set the trigger delay time (picoseconds), hardware binning (normally none), CCD temperature (normally −20 °C), intensifier gain (0 to 255), gate width (picoseconds), 16-bit analog-to-digital conversion rate (normally set to 500 K Hz so that only one of the two existing analog-to-digital circuits is used for all conversions), and the number of images to accumulate and to transfer individual images to digital arrays. Images are accumulated by one's leaving the CCD on and allowing charge to continue to accumulate in individual pixel wells while the intensifier is turned on and off in relation to the *Q*-switch-based trigger and camera settings. A computer program was written to set the region of interest (not used in this study), to control image acquisition and display, and to write 15-bit images to disk. Images were restricted to 15 bits to allow data to be stored as signed integers. For most trials, a set of 30 images were acquired and saved to disk following activation of a single command button. For the first 28 images, the gain was 250, the gate width was 2 ns, and the number of images accumulated was eight. The difference among images was that the trigger delay was incremented 1 ns for each sequential image. The initial trigger delay was set to a fixed value that corresponded to 3 ns before the first sign of a fluorescence response could normally be detected. For the 29th image (low range), the gate width was set to 25 ns, the gate delay was set to be the same as the third sequential image, and the number of images accumulated was reduced from eight to six to maintain consistent intensity levels; the image is comparable with integrating sequential images 3 to 27. For the 30th image (high range), the gate width was set to 20 ns, the gate delay was set to be the same as the 15th sequential image, and the number of images accumulated was again set to eight; the image is comparable with integrating sequential images 15 to 34. In actuality, only 28 sequential images were acquired, so the final (high range) image contains information not available in the sequential images. In a preliminary test, images of treated apples acquired sequentially over 10-min periods showed no evidence of photobleaching.

E. Image Manipulation

A number of computer programs were written to facilitate analyses of images. The first program combined sets of images from 12 apples into a single three-dimensional tray file by use of the ENVI file format in which the data were arranged as 2 apples by 6 apples by 30 images per apple. This program also allows creation of a file that contains location masks for each of the contamination sites. Because the image coordinates are identical for each of the 30 *z*-dimension images, the location file is two-dimensional and encompasses only the 2-apple by 6-apple dimensions of the tray files. The masks consisted of fixed-dimension squares that are manually positioned so that the selected contamination site is centered in the square. The type of contamination site is coded by color. The underlying image on which the squares are placed can be any one of the 30 *z*-dimension images, and one can test the validity of location masks by superimposing the mask file on different *z*-dimension images. Larger masks were used to establish the exact location of apples within images.

Because of memory considerations, separate tray files were created for each of the four quadrants of the camera images, i.e., for each filter wavelength. The images in tray files were registered so that it was necessary to create only a single location file for each set of four related tray files.

A second program allowed creation of combined three-dimensional image files based on tray and location files created by the first program. As each tray file contains images of 12 apples, eight tray files were needed to encompass images of the 96 apples of each type. To allow half the data to be used to develop algorithms and the other half to be used for validity testing, we created combined image files with apple masks and either odd- or even-numbered tray files. Thus combined image files included images from 48 apples arranged as 8 apples by 6 apples; individual apple image segments were 351 by 351 pixels and masks for contamination sites were 25 by 25 pixels.

As the original combined image files contained information based on only a single filter, a program was written to expand the *z* dimension from 30 to 32. The additional space allows inclusion of images, or transformed images, acquired with any filter. As the im-

ages are registered, the addition information allows manipulations such as taking ratios of images acquired with different filters.

F. Image Analyses

A fourth program was written to analyze the combined image files. An image derived from a segment of the combined image based on the mask used to create the combined image, e.g., a single apple image, can be analyzed by use of image manipulations (e.g., binning, brightness, contrast, normalization, exponential scaling, linear combination of images, and ratios of two images) and filters (e.g., spatial, geometric, morphological, edge, and threshold).[19] Raw or transformed images can be viewed as images, false-color images, or histograms. One accomplishes automated detection by subjecting an image to a selected series of transformations and then by applying a threshold to the resultant image. All pixels above the threshold and within a selected pixel distance of each other are considered to be from the same site. Classification of sites by treatment is accomplished by one's comparing the centroids of the sites with the centroids of the contamination site masks. A positive match occurs if the centroids are within a selected distance of each other. If enabled, the program records the centroid coordinates and the number of pixels associated with each classified contamination site along with similar information for the largest unclassified, presumably false-positive, site.

A final program tabulates recorded results. The numbers of recorded pixels for each classified contamination site and for the largest unclassified site are compared with a selected classification threshold. If the number of pixels is greater than or equal to the classification threshold, the response is tabulated as a true response. One option is to investigate the effect of changing the classification threshold on the number of contamination sites correctly detected versus the number of false-positive sites detected. For example, all false positives for a particular detection algorithm can be eliminated by one's setting the classification threshold just greater than the largest number of detected pixels for any unclassified contamination site.

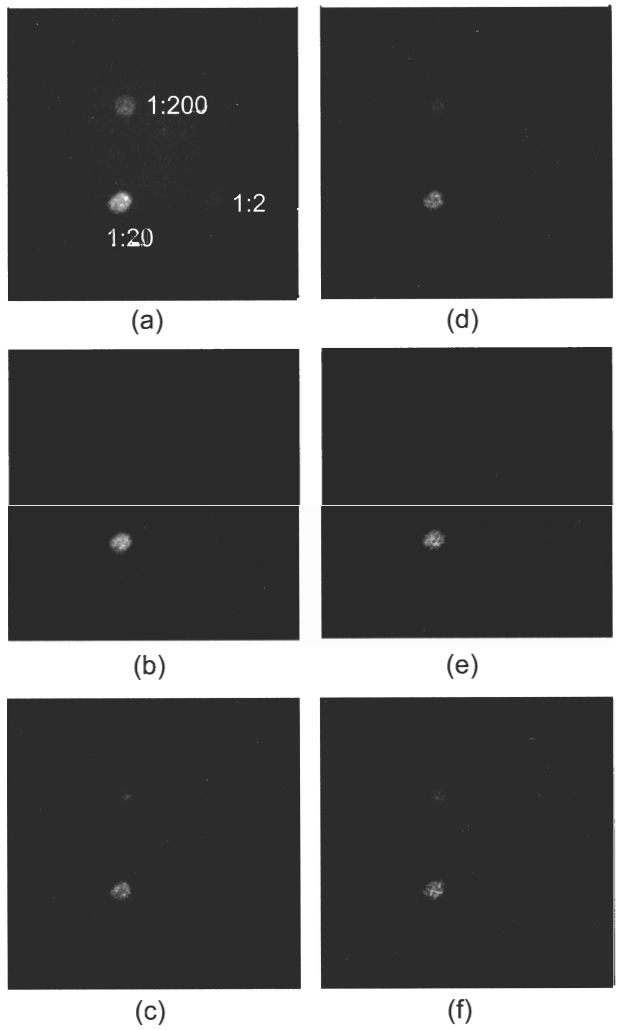

Fig. 2. Images of a representative Red Delicious apple acquired at 682 nm. The gate delay time for sequential images was (a) 10 ns, (b) 12 ns, (c) 14 ns, (d) 16 ns, (e) 18 ns, (f) 20 ns; however, the gate width remained constant at 2 ns. Each image is scaled to its maximum intensity. Locations of areas where the 1:2, 1:20, and 1:200 feces treatments were applied are as indicated. Note that the treated areas are visible at all gate delays, but visibility of the apple decreases as the gate delay increases.

3. Results and Discussion

A. Response Characteristics

As was found in a prior study, the intensity of fluorescence responses did not scale with the concentration of applied feces (Figs. 2 and 3).[17] The measured response for a treated area appears to be a weighted summation of the responses of the feces and of the underlying apple surface. The applied feces can obstruct illumination of the underlying apple surface and potentially reabsorb energy released by the apple surface. In general, the intensity of fluorescence responses in the red bands for 1:2 treatment areas was less than responses for 1:20 treatment areas. For the 1:2 dilution areas, the density of the applied manure probably interfered with both the illumination and the response of the underlying apple surface. For the 1:20 dilution, the applied feces visually appeared to be translucent, and the measured response is probably a summation of the responses of the feces and the underlying apple surface. Given the complexity of these interactions, formal analyses of decay characteristics are beyond the scope of this study. Furthermore, information about theoretical decay characteristics is of little use for designing a commercial detection system as time and cost constraints do not allow for acquisition of sequential images for single apples. For commercial applications, it is more important to look at the relative intensity of responses as a function of potential gate widths and gate delays. For this reason, raw intensity responses by time are shown rather than normalized responses,

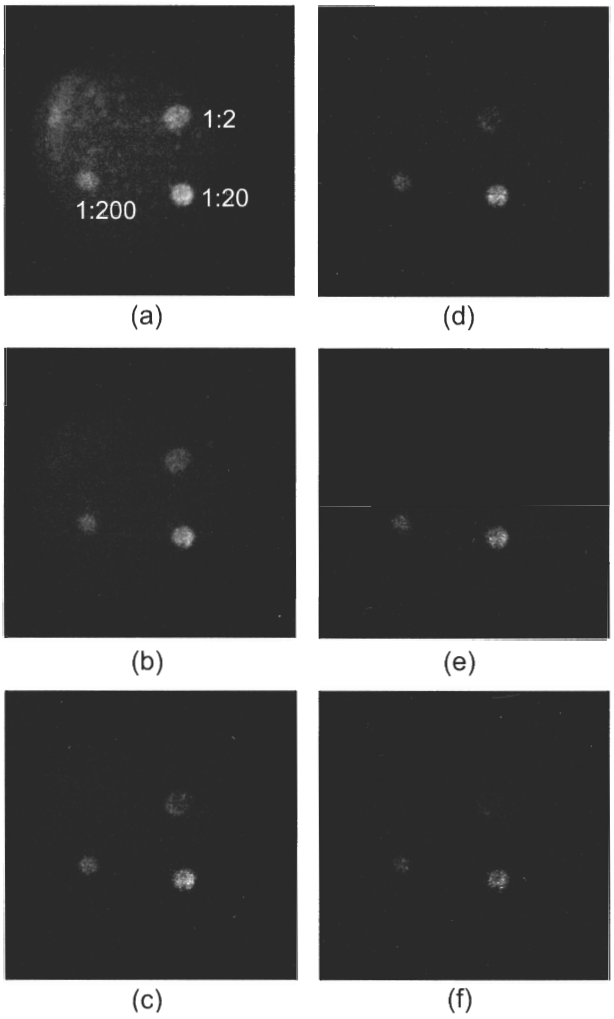

Fig. 3. Images of a representative Golden Delicious apple acquired at 682 nm. The gate delay time for sequential images was (a) 10 ns, (b) 12 ns, (c) 14 ns, (d) 16 ns, (e) 18 ns, (f) 20 ns; however, the gate width remained constant at 2 ns. Each image is scaled to its maximum intensity. Locations of areas where the 1:2, 1:20, and 1:200 feces treatments were applied are as indicated. Note that the treated areas are visible at all gate delays, but visibility of the apple decreases as the gate delay increases.

which would be more appropriate for analyzing decay constants.

B. Detection Parameters

Selection of the wavelengths and bandwidths for filters used in this study was based on demonstrated fluorescence response characteristics of feces and apples. Using hyperspectral imaging techniques, the authors previously demonstrated that ratios of appropriate band images helped to normalize effects due to heterogeneous illumination and that detection of fecal contamination was enhanced when a red-band image was divided by the corresponding blue-band image and, to a lesser extent, by the green-band, image.[13] More recently, ratios of red-band to blue-band images acquired by use of a pulsed UV laser for excitation were found to improve detection of

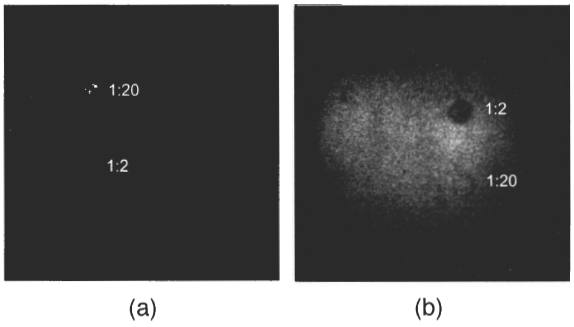

Fig. 4. Images of representative (a) Red Delicious and (b) Golden Delicious apples acquired at 590 nm by using a 10-ns gate delay and a 2-ns gate width. Each image is scaled to its maximum intensity. Locations of areas where feces treatments were applied are as indicated. Note that the 1:2 treated area is brighter than the surrounding apple surface in the image of the Red Delicious apple and that it is darker in the image of the Golden Delicious apple.

1:2 dilutions of feces applied to Red Delicious apples; in contrast, detection of 1:200 dilution sites was better when only red-band images were analyzed.[17] In the current study, use of 417-nm excitation precluded use of a blue (~450-nm) filter. Instead, a broad-bandwidth 590-nm (yellow) filter was used to capture the tail end of the green fluorescence emission spectra. Examples of images acquired with this filter are shown in Fig. 4. Note that the green coloration of Golden Delicious apples resulted in higher-intensity fluorescence responses in the yellow band for untreated apple surfaces compared with Red Delicious apples. As a consequence, for Golden Delicious apples, fluorescence responses in treated areas were lower than responses in untreated areas (Fig. 5). In contrast, for Red Delicious apples, responses for 1:2 dilution treatment sites were greater than responses for untreated areas. The responses of 1:2 dilution treatments are of particular interest as ratio images are most beneficial for detecting high-concentration treatment sites.[17] Ratio images enhance differences between treated and untreated areas when the direction of the relative response of treated to untreated areas in one image is reversed in the second image. Thus ratio images utilizing 590-nm images offer the potential of enhancing detection of fecal contamination on Golden Delicious but not on Red Delicious apples.

The 682-nm filter was chosen for use, as it was the commercially available filter that best matched the primary fluorescence response characteristics of chlorophyll *a*. The 700-nm filter was meant to encompass both the primary and the secondary chlorophyll-*a* fluorescence emission peaks. Examples of images acquired for Red Delicious and Golden Delicious apples with the 682-nm filter are shown in Figs. 2 and 3, respectively. The intensity of responses of treated and untreated areas are shown in Fig. 6. Images acquired with the 700-nm filter were similar and are not shown.

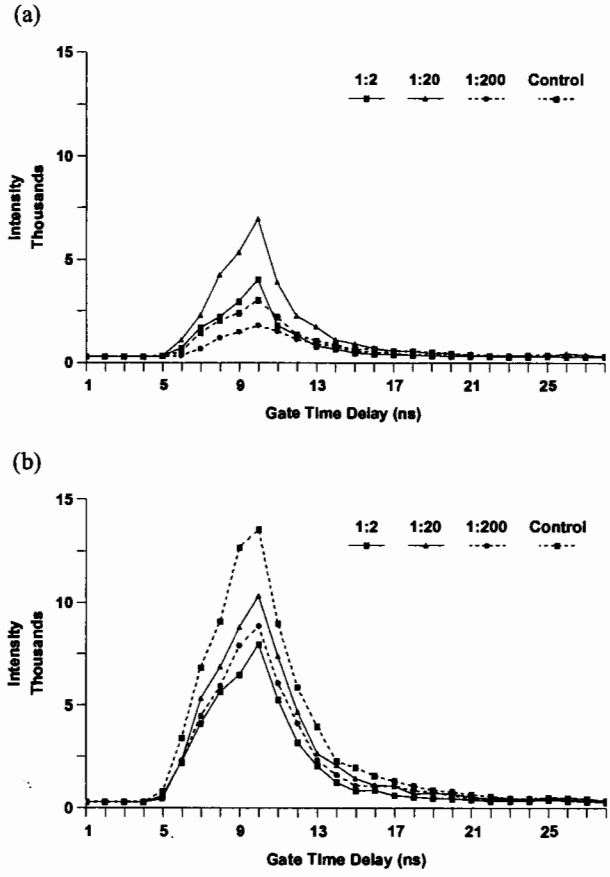

Fig. 5. Average intensities of 9×9 pixel areas for treatment spots on the (a) Red Delicious and (b) Golden Delicious apple images in Fig. 4. Calculated intensities were derived from images acquired by use of gate delay times incremented sequentially by 1 ns; gate width was kept constant at 2 ns. Note the reduced fluorescence responses of the Red Delicious apple compared with the Golden Delicious apple and that, for the Golden Delicious apple, the intensity of the 1:2 treatment spot is consistently lower than the corresponding intensity of the control.

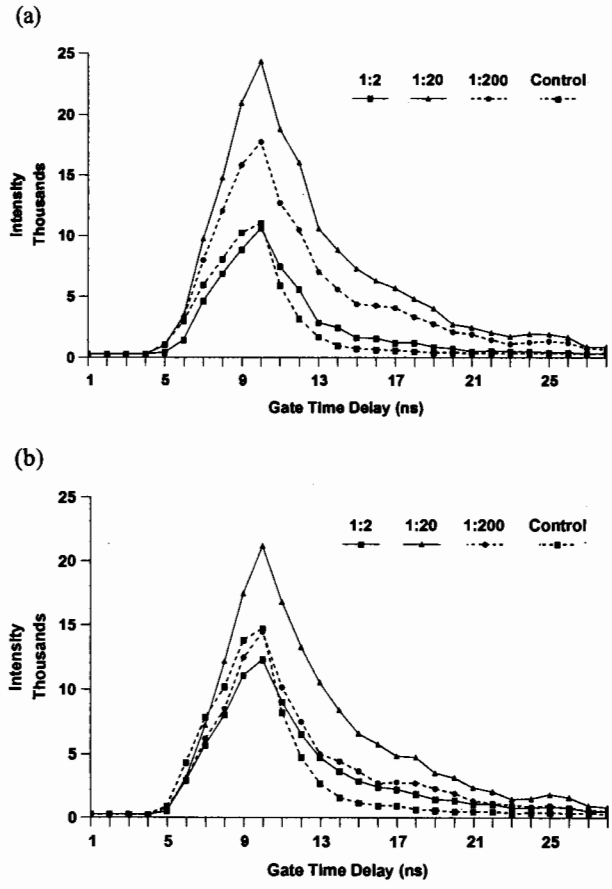

Fig. 6. Average intensities of 9×9 pixel areas for treatment spots on the (a) Red Delicious and (b) Golden Delicious images in Figs. 2 and 3, respectively. Calculated intensities were derived from images acquired by use of gate delay times incremented sequentially by 1 ns; gate width was kept constant at 2 ns. Note that for both (a) Red Delicious and (b) Golden Delicious apples, at 10-ns gate delay, intensities for 1:2 treatment areas are less than corresponding responses for control areas, and, at gate delays greater than 10 ns, intensities for 1:2 treatment areas are greater than corresponding responses for control surfaces.

When one uses a multispectral adapter for imaging, an issue that needs to be addressed is the effective imaging throughput for each of the filters. A broadband filter was used at 590 nm in an attempt to match the intensities of images acquired with the 682- and 700-nm filters. However, owing to low fluorescence yields by use of 417-nm excitation, the intensity of images acquired with the 590-nm filter (Fig. 5) was lower than the intensity of images acquired with the 682- (Fig. 6) or 700-nm filters. Still, the throughput at 590 nm was adequate to provide reasonable sensitivity as pixel counts for regions of interest ranged from 1000 to 20,000. The throughput for the narrowband 730-nm filter was the lowest among all the filters, and pixel intensities for regions of interest ranged from the low hundreds to a few thousand. Although this sensitivity is theoretically adequate to allow effective analyses of images, the images were noisy and grainy. As 730 nm is the secondary emission peak of chlorophyll *a*, the 730 images were similar to the 682- and 700-nm images but were inferior in terms of the signal-to-noise ratio. For these reasons, 730-nm images were not subject to detailed analyses.

It was hypothesized that consideration of differences in the time courses of fluorescence responses for treated and normal apple surfaces might allow for improved detection of feces on apples. The fluorescence responses of both feces and apples in the red band are derived from chlorophyll *a* and related compounds. However, feces are the result of a digestive process designed to break down biological tissue into simpler chemical compounds. It was theorized that this process might alter the time-dependent fluorescence responses of feces compared with intact apples. If so, it might be possible to accentuate differences between corresponding fluorescence responses by use of a pulsed laser for excitation with appropriate selection of the ICCD-camera gate time delay and gate width. Example images in Figs. 2 and 3 clearly demonstrate that the time courses of fluorescence re-

sponses of feces and of normal apple surfaces are different. Graphs of intensity verses gate time delay (Fig. 6) reveal that the fluorescence responses for normal apple surfaces decrease faster with elapsed time compared with areas treated with feces. In contrast, there were no real differences in time-dependent response characteristics at 590 nm (Fig. 5).

The low-range (3 – 27-ns gate window) and high-range (15 – 34-ns gate window) imaging parameters were selected on the basis of preliminary data. The low range was designed to capture the total integrated fluorescence response. The high range was selected to capture the tail of the feces response after the response of untreated apple surface was greatly attenuated. Examination of experimental data suggested that the 12 – 19-ns gate window might also be worth investigating, as this is the range in which responses of treated areas were consistently greater than responses for untreated areas. Images acquired with gate delay times of from 12 to 19 ns were averaged to create the midrange treatment for testing.

Examination of time-sequence images (e.g., Figs. 2 and 3) show that toward the end of the response period for treated areas there was almost no response for untreated apple surfaces. Tests made by use of images acquired with gate delay times greater than 18 ns led to the creation of an additional treatment called the extended range treatment. For both Red Delicious and Golden Delicious apples, the treatment was the sum of images acquired from 20 to 24 ns.

It is interesting to note that the shape of fluorescence responses were similar for both treated and untreated areas in images acquired with the 590-nm filter (Fig. 5). Responses were largely attenuated by 13 ns. This presents a particular problem for constructing a ratio image. Ratios involving high-range, and even midrange, treatments are not useful as there is little or no energy in corresponding images acquired with the 590-nm filter. As an alternative, images acquired with gate delay times from 11 to 13 ns were averaged and designated the short-range treatment. Ratios were calculated for low-range and short-range image sets.

In summary, images acquired with both 682- and 700-nm filters were analyzed in detail with the low-range, short-range, midrange, high-range, and extended range image sets. In addition, ratio images for low-range and short-range data sets were also analyzed. The denominators for all ratio calculations were the corresponding image sets acquired with the 590-nm filter.

C. Detection Algorithms

We tested numerous detection algorithms by applying the algorithms to 48 Red Delicious and 48 Golden Delicious apples. It immediately became apparent that it would be impossible to detect all of the contamination areas with no false positives. For both group of apples, a number of apples showed signs of natural contamination. Examples of images showing natural contamination sites on Red Delicious and Golden Delicious apples are shown in Fig. 7. In most cases, there was no abnormality associated with the natural contamination sites that was visible to the naked eye. In a few cases, the response was associated with what appeared to be a healing wound. An additional clue concerning natural contamination sites is that apples with such sites had a tendency to show early signs of an infection process, including brown areas. However, the detected natural sites did not generally correspond to the potential disease sites. Of course, some of the natural contamination may actually be fecal contamination that occurred prior to harvesting or as a result of splatter during feces application.

Given the existence of the natural contamination sites, trade-offs between detection of artificial and natural contamination sites became a critical issue. In general, the artificial sites were larger than the natural sites. However, if the classification threshold is increased to reduce the number of false positives, the minimum theoretical size of any contamination site that can be detected is increased. Also, raising the threshold too high will reduce the number of artificial contamination sites detected. To better determine the effect of the classification threshold on detecting natural and artificial contamination sites, we sorted the numbers of pixels above the threshold for natural sites from largest to smallest. Then the classification threshold was set sequentially to match these values. For example, if the classification threshold is set to the third largest value, the first two natural contamination sites will be classified as real responses. Empirically, the number of correctly classified artificial sites jumped upward when the threshold was set to match the fifth largest value for natural contamination sites. The natural contamination sites shown in Fig. 7 produce the second or third largest responses, depending on the detection algorithm used, and are always classified as a true response when the classification threshold is set to match the fifth largest pixel count for natural contamination sites.

The pixel count for the fifth largest natural contamination site for the detection algorithm being tested was selected to be the classification threshold for testing of detection algorithms. Although this threshold was derived empirically, the procedure used to select the threshold is reasonable, and it allows direct comparison of different detection algorithms. In addition, the successful application of algorithms derived with the sets of apple test images to the validation image sets, as discussed below, demonstrates the appropriateness of using this methodology.

After numerous trials using the sets of test images, two types of algorithm were selected for further optimization. Both algorithms first transformed the images by use of a linear transform to equalize intensities; the 5% cumulative histogram level was mapped to an intensity of 20, and the 60% histogram level was mapped to an intensity of 100. The maximum intensity was limited to 1023. For the extended

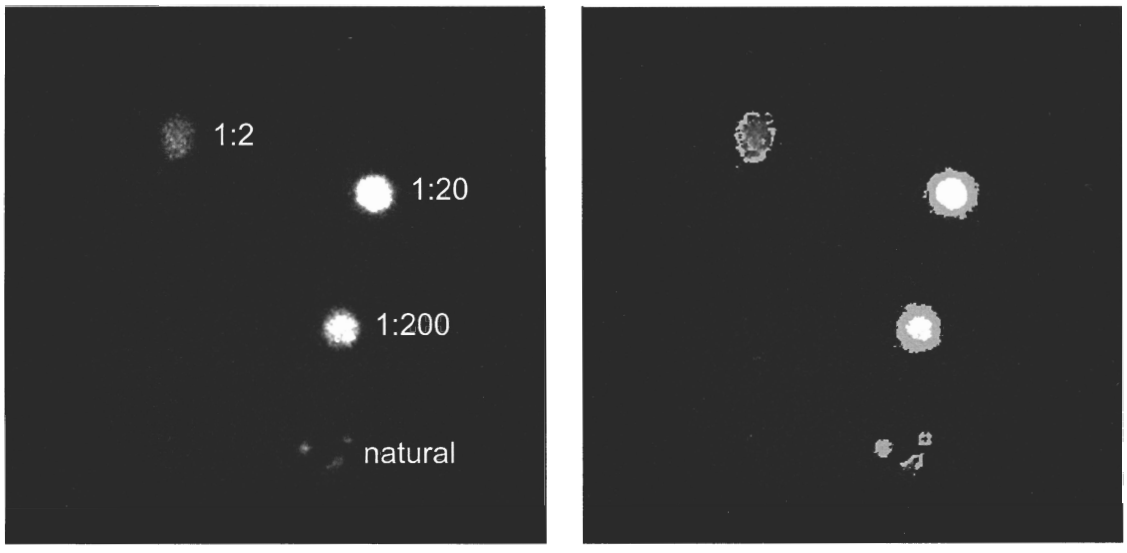

(a)

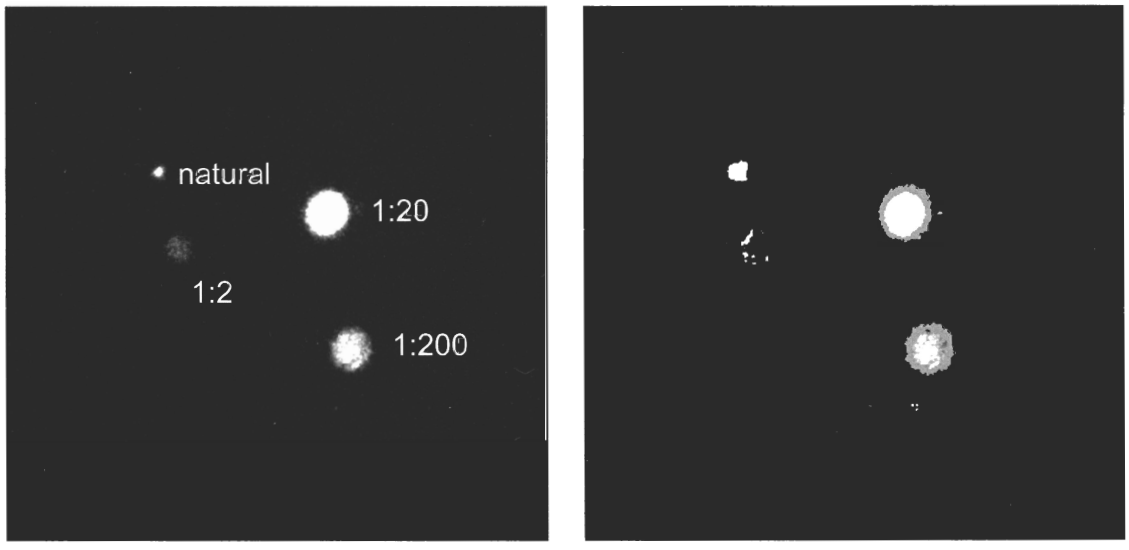

(b)

Fig. 7. Images of (a) Red Delicious and (b) Golden Delicious apples acquired with the 682-nm filter with a gate interval of 15 − 34 ns (high range). Locations of feces treatment sites are as indicated. Images on the left are of the apples before detection, and the images on the right show detected pixels in light gray. The detection algorithm used was based on edge detection, hence the circular aspect of detected areas. The images were selected for presentation due to the natural contamination sites that appear in the images.

range image sets, a simple threshold was applied to the transformed images. The threshold was iterated until the maximum numbers of artificial contamination sites were detected, given that the classification thresholds were set to the pixel count of the fifth largest natural contamination site. For the other image sets, a 5×5 Prewitt filter[19] was applied to take advantage of the observation that contaminated areas were brighter than the surrounding untreated apple surface, regardless of variation in pixel intensities of untreated areas across an apple surface. The authors have previously demonstrated that edge detection can be a sensitive method for detecting fecal contamination on apples.[17] The only real problem with the use of edge detection is the tendency to detect the actual edges of the apple or small increases in pixel intensities at the edges of apples. To alleviate this problem, we set the minimum intensity of images just below the pixel intensity of apple edges prior to applying edge detection.

One additional step was necessary for analyzing ratio images. Registration of images was not perfect, which commonly resulted in enhanced detection of the actual edges of apples. To address this problem, we binned the images used to calculate ratios 2×2 prior to ratio calculations.

Detection results for Red Delicious and Golden Delicious apples are in Tables 1 and 2, respectively. The optimized algorithms used to create Tables 1 and 2 were applied to the second sets of apples without

Table 1. Number of Red Delicious Apples from a Total of 48 Apples for Testing, for which the Contamination Site Was Successfully Detected by Filter (682 or 700 nm), Treatment (1:2, 1:20, and 1:200 Dilutions of Dairy Feces), and Image Set[a]

	682 nm			700 nm		
Gate Aperture	1:2	1:20	1:200	1:2	1:20	1:200
Low range (3–27)[b]	13	48	26	11	48	32
High range (15–34)	31	48	46	22	48	46
Midrange (12–19)	26	48	45	23	48	46
Short range (11–13)	16	48	33	14	48	40
Ratio short range[c]	4	27	18	4	34	35
Extended range (20–24)	40	48	48	32	47	48

[a]Image sets relate to the gate timing of the ICCD camera. Algorithms used for detection were iteratively optimized for each image set.
[b]Numbers in parentheses correspond to the window gate in nanoseconds.
[c]For ratio images, images in the indicated image set were divided by corresponding images acquired with the 590-nm filter.

Table 3. Number of Red Delicious Apples from a Total of 48 Apples for Validation, for which the Contamination Site Was Successfully Detected by Filter (682 or 700 nm), Treatment (1:2, 1:20, and 1:200 Dilutions of Dairy Feces), and Image Set[a]

	682 nm			700 nm		
Gate Aperture	1:2	1:20	1:200	1:2	1:20	1:200
Low range (3–27)[b]	10	47	22	5	46	31
High range (15–34)	32	48	46	20	48	46
Midrange (12–19)	22	48	44	17	47	44
Short range (11–13)	18	48	32	14	48	40
Ratio short range[c]	4	37	21	4	39	30
Extended range (20–24)	40	48	47	29	47	48

[a]Image sets relate to the gate timing of the ICCD camera. The optimized detection algorithms derived for Table 1 were applied to these image sets for validation.
[b]Numbers in parentheses correspond to the window gate in nanoseconds.
[c]For ratio images, images in the indicated image set were divided by corresponding images acquired with the 590-nm filter.

modification to test the validity and robustness of the optimized detection algorithms (Tables 3 and 4). The results for both sets of Red Delicious and for both sets of Golden Delicious apples were essentially identical, thus validating the methodology used to derive the detection algorithms.

For Red Delicious apples, the best overall image set for detection of artificial contamination sites was the extended range image set. However, only 40 of the 48 apples contaminated with the 1:2 dilution of feces were detected for both testing and validation image sets (Tables 1 and 3). In a prior study that used a UV pulsed laser, detection of high-concentration treatment sites by use of only red-band images was also found to be difficult.[17] However, when ratio images were constructed by dividing red-band images by corresponding blue-band images, detection of most 1:2 dilution contamination sites was successful. The results in this study using only enhanced range red-band images were superior to the results of the previous study when only red-band images were used for detection. Unfortunately, blue-band images were not available in this study owing to the use of 417-nm excitation. Another advantage of the extended range image set was the enhanced ability to detect the 1:200 dilution treatment sites. Enhanced detection of this low-concentration treatment was

Table 2. Number of Golden Delicious Apples from a Total of 48 Apples for Testing, for which the Contamination Site Was Successfully Detected by Filter (682 or 700 nm), Treatment (1:2, 1:20, and 1:200 Dilutions of Dairy Feces), and Image Set[a]

	682 nm			700 nm		
Gate Aperture	1:2	1:20	1:200	1:2	1:20	1:200
Low range (3–27)[b]	36	46	32	31	46	34
High range (15–34)	37	48	42	29	48	41
Midrange (12–19)	35	48	34	26	46	37
Short range (11–13)	40	48	28	32	46	34
Ratio low range[c]	46	46	18	43	47	26
Ratio short range	46	48	19	41	47	22
Extended range (20–24)	31	44	38	21	41	36
Combined low range[d]	47	46	33	47	47	38
Combined short range	47	48	34	45	48	36

[a]Image sets relate to the gate timing of the ICCD camera. Algorithms used for detection were iteratively optimized for each image set.
[b]Numbers in parentheses correspond to the window gate in nanoseconds.
[c]For ratio images, images in the indicated image set were divided by corresponding images acquired with the 590-nm filter.
[d]Results for combined image sets are the union of detection results for corresponding normal and ratio image sets.

Table 4. Number of Golden Delicious Apples from a Total of 48 Apples for Validation, for which the Contamination Site Was Successfully Detected by Filter (682 or 700 nm), Treatment (1:2, 1:20, and 1:200 Dilutions of Dairy Feces), and Image Set[a]

	682 nm			700 nm		
Gate Aperture	1:2	1:20	1:200	1:2	1:20	1:200
Low range (3–27)[b]	35	46	24	29	47	27
High range (15–34)	29	48	41	22	46	38
Midrange (12–19)	32	48	36	17	47	34
Short range (11–13)	37	48	30	25	48	33
Ratio low range[c]	45	48	12	45	45	13
Ratio short range	45	45	13	36	47	16
Extended range (20–24)	23	45	35	12	42	35
Combined low range[d]	46	46	24	45	48	36
Combined short range	46	48	30	47	47	38

[a]Image sets relate to the gate timing of the ICCD camera. The optimized detection algorithms derived for Table 2 were applied to these image sets for validation.
[b]Numbers in parentheses correspond to the window gate in nanoseconds.
[c]For ratio images, images in the indicated image set were divided by corresponding images acquired with the 590-nm filter.
[d]Results for combined image sets are the union of detection results for corresponding normal and ratio image sets.

also seen for the high-range and the midrange image sets.

The optimal situation might be to use UV excitation to allow acquisition of blue-band images for calculation of ratios for detection of high-concentration contamination sites. However, using the extended range is also a viable option. Water baths are used commercially to remove apples from crates prior to processing, and apples are commonly brushed clean as they are removed from the water bath. The authors have demonstrated that the fluorescence responses of sites contaminated with high concentrations of feces are enhanced after the apples are washed and brushed.[17] In addition, use of the extended range for imaging offers the benefits of enhanced detection of low-concentration contamination sites and a simple detection scheme, which consists of a linear mapping of intensities followed by a simple threshold.

The most successful detection scheme for Golden Delicious apples utilized the short-range image set (Tables 2 and 4). The timing parameters for this image set were selected to meet two criteria: (1) the intensities for treated areas were greater than for untreated areas in red-band images, and (2) the reverse was true for corresponding yellow-band images. By analyzing both red-band images and ratios of red-band to yellow-band images and by taking the union of detection results, it was possible to detect essentially all of the 1:2 and 1:20 treatment sites for both 682- and 700-nm image sets; however, detection of 1:200 treatment sites was superior when the 700-nm image sets were analyzed. This is the only situation in which images acquired at 700 nm appeared to produce better detection results compared with 682 nm. In any case, the most 1:200 dilution sites were detected when the high-range image set was analyzed. Still, current results are good and the detection algorithms based on the short-range timing parameters might prove useful in a commercial environment.

4. Conclusions

In this study the use of time-resolved imaging allowed for the optimization of imaging parameters for the detection of dairy feces artificially applied to apples. It was determined that fluorescence responses of untreated apple surfaces at 682, 700, and 730 nm attenuated to low intensity levels faster with time (nanosecond time scale) than responses of areas treated with feces. At 590 nm, the shapes of responses for treated and untreated areas were similar. For Red Delicious apples, optimal detection of contamination sites utilized images acquired with the 682-nm filter with the camera exposure parameters set so the fluorescence response of the apple surface was largely gone, but there was still some response from the areas treated with feces. For Golden Delicious apples, optimal detection utilized images acquired with the 682- and 590-nm filters, with the camera exposure parameters set so that images were taken during a time period in which responses of treated areas exceeded responses of untreated areas in images acquired at 682 nm and responses were visible in images taken at 590 nm. Excellent overall detection resulted when both the 682-nm images and the ratio of the 682- to 590-nm images were analyzed and the detection results combined. These findings demonstrate that consideration of the timing of fluorescence responses to pulsed-laser excitation can enhance detection of feces on apples and can facilitate development of commercial systems to detect apples contaminated with feces.

References

1. Food and Drug Administration, "Hazard analysis and critical control point (HAACP); procedures for the safe and sanitary processing and importing of juices," Fed. Regist. **66,** 6137–6202 (2001).
2. Food Safety and Inspection Service, U.S. Department of Agriculture, "Verification of procedures for controlling fecal material, ingesta, and milk in slaughter operations," Directive 6420.2, http:www.fsis.usda.gov (2004), pp. 1–14.
3. G. L. Armstrong, J. Hollingsworth, and J. G. Morris, Jr., "Emerging foodborne pathogens: *Escherichia coli* O157:H7 as a model of entry of a new pathogen into the food supply of the developed world," Epidemiol. Rev. **18,** 29–51 (1996).
4. R. L. Buchanan and M. P. Doyle, "Foodborne disease significance of *Escherichia coli* O157:H7 and other enterohemorrhagic *E. coli*," Food Technol. **51,** 69–76 (1997).
5. R. E. Brackett, "Incidence, contributing factors, and control of bacterial pathogens in produce," Postharv. Biol. Technol. **15,** 305–311 (1999).
6. P. S. Mead, L. Slutsker, V. Dietz, L. F. McCaig, J. S. Bresee, C. Shapiro, P. M. Griffin, and R. V. Tauxe, "Food-related illness and death in the United States," Emerg. Infect. Dis. **5,** 607–625 (1999).
7. Centers for Disease Control and Prevention, "Outbreaks of *Escherichia coli* O157:H7 infection and cryptosporidiosis associated with drinking unpasteurized apple cider—Connecticut and New York, October 1996," Morb. Mortal. Wkly Rep. **46,** 4–8 (1997).
8. P. J. Harris and R. D. Hartley, "Detection of bound ferulic acid in cell walls of the Gramineae by ultraviolet fluorescence microscopy," Nature **259,** 508–510 (1976).
9. J. Hewett, V. Nadeau, J. Ferguson, H. Moseley, S. Ibbotson, J. W. Allen, W. Sibbett, and M. Padgett, "The application of a compact multispectral imaging system with integrated excitation source to *in vivo* monitoring of fluorescence during topical photodynamic therapy of superficial skin cancers," Photochem. Photobiol. **73,** 278–282 (2001).
10. H. H. Kim, "New algae mapping technique by the use of an airborne laser fluoresensor," Appl. Opt. **12,** 1454–1459 (1973).
11. V. Tassetti, A. Hajri, M. Sowinska, S. Evrard, F. Heisel, L. Q. Cheng, J. A. Mieh, J. Marescaux, and M. Aprahamian, "*In vivo* laser-induced fluorescence imaging of a rat pancreatic cancer with pheophorbide-*a*," Photochem. Photobiol. **65,** 997–1006 (1997).
12. E. W. Chappelle, J. E. McMurtrey, and M. S. Kim, "Identification of the pigment responsible for the blue fluorescence band in laser-induced fluorescence (LIF) spectra of green plants, and the potential use of this band in remotely estimating rates of photosynthesis," Remote Sens. Environ. **36,** 213–218 (1991).
13. M. S. Kim, A. M. Lefcourt, Y. R. Chen, I. Kim, K. Chao, and D. Chan, "Multispectral detection of fecal contamination on apples based on hyperspectral imagery. II. Application of fluorescence imaging," Trans. ASAE **45,** 2027–2038 (2002).

14. D. Krizek, E. M. Middleton, R. Sandhu, and M. S. Kim, "Evaluating UV-B effects and EDU protection in cucumber leaves using fluorescence images and fluorescence emission spectra," J. Plant Physiol. **158,** 41–53 (2001).
15. M. Sowinska, T. Decker, C. Eckert, F. Heisel, R. Valcke, and J. Miehe, "Evaluation of nitrogen fertilization effect on apple-tree leaves and fruit by fluorescence imaging," in *Advances in Laser Remote Sensing for Terrestrial and Hydrographic Applications*, R. M. Narayanan and J. E. Kalshoven, eds., Proc. SPIE **3382,** 100–111 (1998).
16. M. S. Kim, A. M. Lefcourt, and Y. R. Chen, "Optimal fluorescence excitation and emission bands for detection of fecal contamination," J. Food Protection **66,** 1198–1207 (2003).
17. A. M. Lefcourt, M. S. Kim, and Y. R. Chen, "Automated detection of fecal contamination of apples by multispectral laser-induced fluorescence imaging," Appl. Opt. **42,** 3935–3943 (2003).
18. M. S. Kim, A. M. Lefcourt, and Y. R. Chen, "Multispectral laser-induced fluorescence imaging system for large biological samples," Appl. Opt. **42,** 3927–3934 (2003).
19. A. R. Weeks, Jr., *Fundamentals of Electronic Image Processing* (SPIE, Bellingham, Wash., 1996).